Integrated Artificial Intelligence and Physics-Based Modeling for Long-Term Cascaded Hydropower Scheduling under Extreme Heat Events

Maryam Baghkarvasef, *Student Member, IEEE,* and Masood Parvania, *Senior Member, IEEE*

***Abstract*—The operation of hydropower plants are significantly challenged by extreme heatwave events. This paper integrates artificial intelligence and a physics-based model to introduce an efficient long-term scheduling framework aimed at maximizing hydropower generation during extreme heat events. The water values derived from the proposed long-term scheduling model can be used in developing effective strategies for short-term hydropower scheduling. A physics-based evaporation model (PEM), which captures key land-atmosphere interactions, is developed to account for significant variations in reservoir evaporation rates during extreme heat events. A multivariate long short-term memory (M-LSTM) forecasting model is also utilized to predict the key input parameters required for both the PEM and the long-term scheduling problem. A regression-based machine learning algorithm is also utilized to estimate the hydropower production function, which enables linear integration of the nonlinear and nonconvex behavior of hydropower plant in the mixed-integer linear formulation of the scheduling problem. The proposed model is applied to a case study of eleven cascaded hydropower units located on the Columbia river. The numerical results demonstrate that the proposed long-term scheduling model effectively manages reservoir operations, mitigating the adverse impacts of extreme heat events on hydropower generation and operator profitability.**

***Index Terms*—Extreme heat events, hydropower, long-term scheduling, artificial intelligence, physics-based evaporation model.**

NOMENCLATURE

Indices and Sets

h, $\mathcal{H}$	Index and set of hydropower plants
t, $\mathcal{T}$	Index and set of time (hours of a day)
n, $\mathcal{N}$	Index and set of days
i, $\mathcal{I}_h$	Index and set of upstream hydropower plants

Variables

$q^{in}_{n,h,t}, q^{out}_{n,h,t}$	Inflow, Outflow $[\mathrm{m^3\,s^{-1}}]$
$q^{S}_{n,h,t}, q^{B}_{n,h,t}$	Spillage, Bypass flow $[\mathrm{m^3\,s^{-1}}]$
$q^{net}_{n,h,t}, q^{D}_{n,h,t}$	Net, Discharge flow $[\mathrm{m^3\,s^{-1}}]$
$p^{H,D}_{n,t}$	Power sold in day-ahead market [MW]
$p^{H}_{n,h,t}$	Hydropower generation [MW]
$V_{n,h,t}$	Storage volume $[\mathrm{m^3}]$
$H^{D}_{n,h,t}$	Hydraulic head [m]
$Z^{f}_{n,h,t}, Z^{t}_{n,h,t}$	Forebay, Tail water level [m]
$l^{H,LS}_{n,t}$	Load shedding [MW]

Binary variables

$U_{n,h,t}$	Commitment indicator
$u^{c}_{n,h,t,k}$	Cluster selection indicator
$S^{u}_{n,h,t}, S^{d}_{n,h,t}$	Startup, Shutdown of hydropower plant

Parameters

η_h	Turbine efficiency
ρ	Density of Water $[\mathrm{kg\,m^{-3}}]$
g	Acceleration due to Gravity $[\mathrm{m\,s^{-2}}]$
k_c	Crop coefficient
$q^{W}_{n,h,t}$	Water demand $[\mathrm{m^3\,s^{-1}}]$
$I_{n,h,t}$	Natural inflow to the reservoir $[\mathrm{m^3\,s^{-1}}]$
α^{b}	Albedo
α	Aerodynamic coefficient
α^{e}	Empirical coefficient
a^{c}	Unit conversion coefficient
β	Empirical coefficient
$R_{n,h,t}$	Net radiation $[\mathrm{MJ\,m^{-2}}]$
$G_{n,h,t}$	Ground heat flux $[\mathrm{MJ\,m^{-2}}]$
$T_{n,h,t}, T^{d}_{n,h,t}$	Temperature, Dew point temperature $[^\circ\mathrm{C}]$
$u^{r}_{n,h,t}$	Hourly u component of wind speed measured at the height of the reservoir $[\mathrm{m\,s^{-1}}]$
$u^{s}_{n,h,t}$	Hourly u component of wind speed measured at the height of 2 meters $[\mathrm{m\,s^{-1}}]$
e^{0}	Reference saturation vapor pressure [kPa]
$e^{s}_{n,h,t}, e^{a}_{n,h,t}$	Saturation, Actual vapor pressure [kPa]
$\Delta_{n,h,t}$	Slope of the vapor pressure-temperature curve $[\mathrm{kPa\,^\circ C^{-1}}]$
δ	Time interval [s]
γ	Psychrometric constant $[\mathrm{kPa\,^\circ C^{-1}}]$
ϵ^{m}	Ratio of molecular weight of water vapor $[\mathrm{MJ\,kg^{-1}\,^\circ C^{-1}}]$
$A_{n,h,t}$	Surface area of reservoir $[\mathrm{m^3}]$
$E_{n,h,t}$	Reservoir evaporation volume $[\mathrm{m^3}]$
$P^{v}_{n,h,t}$	Reservoir precipitation volume $[\mathrm{m^3}]$
a	Conversion factor
b	Scaling factor
c	Temperature conversion factor
$E^{ref}_{n,h,t}$	Reference reservoir evaporation [mm]
$P^{ref}_{n,h,t}$	Reference reservoir precipitation [mm]
L^{v}	Latent heat of vaporization $[\mathrm{MJ\,kg^{-1}}]$

This paper is based upon work supported by the National Science Foundation under Grant Number 2330582.

M. Baghkarvasef and M. Parvania are with the Department of Electrical and Computer Engineering at the University of Utah, Salt Lake City, UT, 84112 USA (e-mails: {maryam.baghkarvasef, masood.parvania}@utah.edu).

$E^R_{n,h,t}$	Radiative evaporation [$\mathrm{mm^3\,h^{-1}}$]
$E^A_{n,h,t}$	Aerodynamic evaporation [$\mathrm{mm^3\,h^{-1}}$]
T^0	Reference temperature [°C]
Z^0	Roughness length [m]
K^0	Reference height [m]
K^r	Reservoir height [m]
Ψ	Empirical vapor pressure coefficient
$S^p_{n,h,t}$	Surface pressure [kPa]
C^p	Specific heat [$\mathrm{MJ\,kg^{-1}\,°C}$]
$\lambda^D_{n,t}$	Electricity price [$/MWh]
$\lambda^C_{n,t}$	Contract price [$/MWh]
$P^{H,C}_{n,t}$	Contracted power [MW]
c^B_h	Penalty for bypassed water [$/$\mathrm{m^3}$]
c^S_h	Penalty for spilled water [$/$\mathrm{m^3}$]
c^{SU}_h, c^{SD}_h	Startup/Shutdown cost [$]
$w^v_{n,h,t}$	Water value [$/$\mathrm{m^3}$]
$SW^{\downarrow}_{n,h,t}$	Shortwave down radiation [$\mathrm{J\,m^{-2}}$]
$LW^{\uparrow}, LW^{\downarrow}$	Up/down thermal radiation [$\mathrm{J\,m^{-2}}$]
$\overline{q^D_h}$,$\underline{q^D_h}$	Max/min discharge limits [$\mathrm{m^3\,s^{-1}}$]
$\overline{q^B_h}$,$\underline{q^B_h}$	Max/min bypass limits [$\mathrm{m^3\,s^{-1}}$]
$\overline{q^S_h}$,$\underline{q^S_h}$	Max/min spillage limits [$\mathrm{m^3\,s^{-1}}$]
$\overline{V^H_h}$,$\underline{V^H_h}$	Max/min storage volume limits [$\mathrm{m^3}$]
$\overline{P_h}$,$\underline{P_h}$	Max/min hydropower generation [MW]
$\overline{H^D_h}$, $\underline{H^D_h}$	Max/min hydraulic head limits [m]

I. Introduction

A. Motivation

HEATWAVE events are increasing in frequency, severity, and duration [1], causing heightened power demand and diminished power production, which presents a significant challenge to power grid resilience. On the power demand side, elevated temperatures associated with heatwaves lead to a significant increase in energy consumption, primarily driven by the heightened use of air conditioners for cooling purposes [2]. This increase in demand often translates into higher electricity prices and an increased risk of power outages. On the power production side, heatwaves affect nuclear, coal, and gas-fired power plants that depend on large volumes of water for cooling, as elevated water temperatures reduce cooling efficiency and impair power generation. Heatwaves also impact renewable energy generation and efficiency, further lowering energy production. This complex interplay between rising demand, falling supply and strained infrastructure highlights the challenges power systems face during heatwaves [3].

Hydropower accounted for 29% of the U.S. renewable electricity in 2022, supplying over 70% of the Northwest's electricity, while providing long duration storage capacity that is crucial for ensuring system reliability during extreme weather events [4]. Unlike traditional fuel-based power plants, hydropower's capacity is dependent on reservoir water levels, which fluctuate due to weather conditions [5]. Heatwave events increase water demand for municipal and irrigation purposes while simultaneously reducing water availability due to higher evaporation rates [6]. For instance, annual reservoir evaporation can account for approximately 5-10% of the total storage capacity in the western U.S. [7]. Altered precipitation patterns further exacerbate water scarcity, significantly decreasing water capacity. This leads to hydropower shortages, necessitating greater dependence on other renewable energy sources and potentially fossil fuels as energy demand rises with increasing temperature [8]. When the supply of hydropower is low, the revenue for hydropower plants, which sell their electricity to the grid or to customers through various mechanisms, also decreases. For instance, between 2018 and 2021, federal hydropower plants in the Southwest experienced a 20% drop in revenue compared to previous averages, primarily due to decreased sale volumes brought on by drought conditions. Similarly, in 2021, drought conditions in the Pacific Northwest led to a 14% reduction in hydropower generation. In summary, extreme heat events can lead to lower hydropower sales volumes due to limited water availability in storage.

B. Literature Review

Various studies have employed diverse modeling approaches to explore the effects of heatwaves on different facets of power systems. The model in [9] translate heatwave vulnerability into a feeder level metric and embed it in a distribution network model to guide distributed energy resources investments that reduce overheating risk for the most vulnerable customers. A model to optimally site and size cost-effective solar-battery resilience hubs that maintain cooling and power during heatwave outages is presented in [10]. The work in [11] presents an operational strategy for transmission systems during heatwave conditions, accounting for the influence of hourly temperature variations on load patterns, capacity and efficiency of power sources and transmission lines. Heatwaves not only impose stress on power infrastructure and the capacity of power generation units but also contribute to increased costs associated with power generation. In addressing these challenges, a production cost model is developed in [12] that considers the impact of heatwaves on power grid operation and incorporates temperature-dependent loads and generators. Another study in [13] found that heatwaves increase the electricity prices by 11% on average, and more during peak demand, due to the reduced production capacity of thermoelectric power plants that depend on cooling water.

Hydropower generation is also significantly affected by changing weather; therefore, robust hydropower scheduling is essential. In this regard, authors in [14] formulate a stochastic continuous-time hydro-thermal coordination model that balances wind power uncertainty across cascaded hydropower plants and thermal units. A model for coordinated scheduling of cascaded hydro and thermal plants under sequential heavy precipitation is proposed in [15] to enhance the power system resilience. Long-term scheduling of resources emerges as a crucial strategy to address the complex interplay between extreme heat events and power system operations. By extending the scheduling horizon, operators can better anticipate and mitigate the impacts of extreme climate conditions and ensure a reliable and efficient operation. In this regard, authors in [16] develop a long-term complementary scheduling model for hydro-wind-solar systems under extreme drought conditions. A framework is proposed in [17] to analyze long-term impacts

of climate change on hydropower generation in Brazil using multi-stage stochastic optimization. The authors in [18] derive steady-state operating policies for distinct climate regimes (dry, normal, wet) to optimize long-term hydropower and irrigation supply. The study in [19] analyzes the impacts of climate change on hydropower generation, electricity demand, and greenhouse gas emissions, with a focus on long-term scheduling and compound extremes such as droughts and heatwaves. A hydrologically-driven methodology for assessing the adaptive capacity of multi-reservoir water resource systems in the context of long-term hydrological persistence under climate change is proposed in [20]. An efficient water level optimal control method for long-term hydropower scheduling is proposed in [21], which considers reservoir evaporation and leakage losses. A model is presented in [22] for hydrothermal scheduling that incorporates head-dependent hydropower production and considers evaporation as a linear function of average reservoir storage.

Long-term forecasting is essential for identifying seasonal patterns and trends in water availability, which play a crucial role in long-term hydropower scheduling [23]. Authors in [24] evaluate encoder-decoder models for long-term reservoir inflow forecasting, identifying regular long short-term memory (LSTM) with 16 nodes as the optimal model, outperforming statistical models like seasonal auto-regressive integrated moving average and vector auto-regression. A semi-distributed hydrological model is used in [25] for river flow forecasting. A novel ensemble forecasting model for long-term hydropower forecasting is proposed in [26] that combines auto-regressive integrated moving average (ARIMA) and bidirectional LSTM (BiLSTM) models. Authors in [27] propose a multivariate probabilistic forecasting framework using vector autoregressive integrated moving average (VARIMA) and dynamic copulas to capture the linear and nonlinear relationships in monthly runoff and wind speed data, integrating these forecasts into a stochastic optimization model for the long-term joint dispatch of a hydro-wind hybrid system. A novel convolutional neural network (CNN)-BiLSTM model combined with transfer learning for forecasting power generation in run-of-the-river hydropower plants is presented in [28]. LSTM is also utilized in [29] to develop an inflow prediction model aimed at enhancing long-term hydropower scheduling.

Despite significant advancements in hydropower scheduling models, several research gaps remain unaddressed. While most studies acknowledge the increasing frequency of compound climate events, e.g., droughts and heatwaves, the operational strategies for mitigating these impacts on hydropower generation are not fully explored. Although the literature has examined the weather impact on long-term hydropower scheduling, the existing studies are often limited to monthly resolutions, which do not capture short-term variations, including hourly fluctuations in demand, price, and temperature, even though these variations are critical for addressing operational challenges. In addition, other studies have evaluated system-level impacts, e.g., [17], but they often rely on simplified models that aggregate individual hydropower plants, overlooking plant-specific operational dynamics. Further, the literature on hydropower modeling lacks both detailed representation and effective linearization of hydropower production function for reducing the computational complexity of long-term scheduling. Although evaporation is acknowledged as a critical factor influencing water balance, its treatment is often oversimplified, relying on linear models that fail to account for spatial variations across basins or the complexity of watershed dynamics. Moreover, the literature predominantly rely on forecasting reservoir inflows alone, overlooking other essential parameters that could enhance the accuracy of hydropower scheduling.

C. Contributions and Paper Structure

With increasing concern over extreme weather events, integrating land-atmosphere interactions into hydropower modeling is essential for more accurate hydropower operations. In this context, accurately representing evaporation trends during periods of drought or heatwaves is crucial, as it enhances the effectiveness of long-term hydropower scheduling. This paper focuses on the specific implications of heatwaves that affects the hydropower generation, and develops a framework that leverages machine learning to model the hydropower operation and forecast the necessary inputs for long-term scheduling problem more accurately. More specifically, the key contributions of this paper are as follows:

- A comprehensive long-term hydropower scheduling framework is developed that enables hydropower operators to optimize their self-scheduling strategies to participate in the day-ahead energy market. The derived water values from the long-term scheduling problem can be leveraged to improve short-term scheduling decisions, ensuring that hydropower operations are both resilient and economically optimized in the face of variable market and weather conditions.
- A physics-based evaporation model (PEM), capturing land-atmosphere interactions, is integrated in the long-term scheduling problem to accurately model the evaporation rates from hydropower reservoirs.
- A multivariate LSTM (M-LSTM) forecasting model is employed to predict the key input parameters required for both PEM and the long-term scheduling problem.

The remainder of this paper is structured as follows: Section II provides on the problem description and Section III outlines the formulation of the proposed long-term scheduling problem. The case study based on the Columbia river basin is presented in Section IV, and Section V provides the conclusions.

II. Problem Description

This section provides the problem description, highlighting the importance of proposed long-term hydropower scheduling framework integrated with PEM.

A. Hydropower Market Mechanism

Hydropower is marketed through various mechanisms depending on the region and the regulatory framework, including long-term power purchase agreements, short-term bilateral contracts, or participation in day-ahead and real-time wholesale markets. Market operations vary globally; in the U.S.,

electricity markets are managed by Independent System Operators (ISOs) and Regional Transmission Organizations (RTOs), whereas in Europe, they are coordinated by nominated electricity market operators and power exchanges such as European power exchange and Nord Pool. In regions with cascaded hydropower plants in the U.S., Power Marketing Administrations (PMAs) manage the sale and dispatch of hydropower generation [30]. By pooling resources from multiple cascaded hydropower systems, PMAs aim to optimize collective benefits from day-ahead market participation. For instance, the Bonneville Power Administration (BPA), a prominent PMA in the Northwestern U.S., manages extensive hydropower resources in the Columbia River Basin, addressing the complexities of marketing wholesale electricity produced by 31 federal hydroelectric projects. In addition to participating in electricity markets, BPA and other PMAs sell power directly to publicly and privately owned utilities under long-term contracts. Their primary objective is to meet these contractual obligations while strategically marketing any surplus generation capacity in the day-ahead market to maximize overall profitability. In Europe, power exchanges like Nord Pool facilitate competitive trading of hydropower across national borders. Despite differences in market operators and hydropower ownership and operations, the day-ahead market structure is present in most regions worldwide. In many day-ahead electricity markets, so-called self-schedulers must submit generation commitments for each hour of the following day, one day in advance. For an optimal generation scheduling and market participation, hydropower operators must accurately forecast key parameters such as electricity prices, inflows, and contracted demand. This highlights the strong need for advanced forecasting and scheduling strategies that equip hydro operators with insights into the profits they can achieve through informed long-term scheduling and strategic participation in the day-ahead electricity markets.

B. Impact of Extreme Heat Challenges on Water Availability and Hydropower Production

The availability of water for electricity generation at each hydropower plant is significantly constrained by the storage capacities of reservoirs and the projected future inflows within the river basins where these reservoirs are located. The effect of high temperatures and heatwaves further complicates this dynamic, potentially reducing water availability due to increased evaporation rates and changing precipitation patterns, which can alter the volume of water stored in reservoirs. Land-atmosphere interactions play a critical role in shaping the intensity, duration, and frequency of heatwaves, directly influencing water availability for hydropower generation [31]. Increased vapor pressure deficit during heatwaves accelerates water loss from both soil and open water bodies, leading to a reinforcing feedback loop of drier conditions and increased evaporation. Quantifying evaporation is particularly challenging due to its dependence on multiple interrelated meteorological variables, including air temperature, humidity, wind speed, solar radiation, and atmospheric pressure. These factors exhibit complex nonlinear interactions, making evaporation patterns difficult to predict with high precision under varying climate conditions. By integrating advanced forecasting techniques with physics-based evaporation models, hydropower operators can optimize water-energy management decisions.

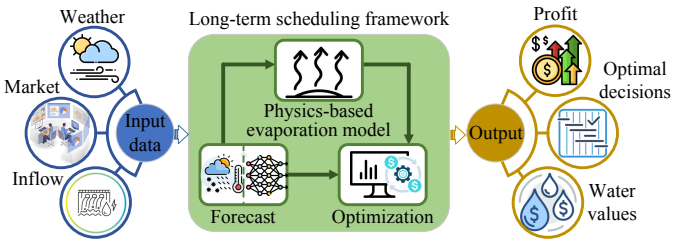

Fig. 1: Diagram of the proposed long-term scheduling framework.

III. Problem Formulation

This section presents the proposed forecasting algorithm, the PEM, and the mathematical framework for long-term hydropower scheduling, as shown in Fig. 1. The input data to the forecasting model includes historical records of weather components, such as temperature, solar radiation, precipitation, as well as market components, e.g., electricity price. It also incorporates hydropower data, such as reservoir inflow and contracted demand. The weather forecasts were incorporated into PEM to estimate the evaporation rates of the reservoir. The evaporation rates, along with forecasted precipitation, inflow, electricity price, and demand, are then fed into the optimization model. The output of the optimization are the optimal decisions, water value estimations, and profit projections gained from day-ahead market participation.

A. The Proposed M-LSTM Forecasting Algorithm

1) Multivariate LSTM forecasting model: LSTM networks improve recurrent neural networks by introducing mechanisms to retain information over long time horizons, thus addressing the vanishing gradient problem. Each LSTM cell comprises multiple gates that regulate the flow of information as detailed in (1)–(6). The forget gate (f_t) in (1) decides how much of the old memory to retain by utilizing the sigmoid activation function (σ) to assign values between 0 and 1, where 1 indicates retaining the information and 0 represents forgetting. The input gate (i_t) regulates which new information from the current input (x_t) is added to the cell state. It also employs the sigmoid activation function to control the flow of new information into the memory as shown in (2). Candidate cell state ($\tilde{c}_t$) in (3), represents the potential new information that can update the cell state. The cell state (c_t) in (4) acts as the memory of the LSTM and combines the previous cell state (c_{t-1}) with the candidate cell state. It uses the hyperbolic tangent activation function ($tanh$) to assign values between 1 and -1, allowing both positive and negative contributions to the information flow. The output gate (o_t) in (5) controls which portion of the updated cell state contributes to the hidden state (n_t^h), which will be passed to the next layer or used for final predictions. The hidden state in (6) is the final output of the LSTM cell and is generated by applying the hyperbolic tangent

function to the updated cell state, followed by modulation through the output gate. These gating mechanisms play a critical role in learning the weights (w^f, w^i, w^c, w^o) and biases (b^f, b^i, b^c, b^o) which are essential for the LSTM's ability to regulate information flow effectively.

$$f_t = \sigma(w^f.[n^h_{t-1}, x_t] + b^f) \quad (1)$$
$$i_t = \sigma(w^i.[n^h_{t-1}, x_t] + b^i) \quad (2)$$
$$\tilde{c}_t = tanh(w^c.[n^h_{t-1}, x_t] + b^c) \quad (3)$$
$$c_t = f_t * c_{t-1} + i_t * \tilde{c}_t \quad (4)$$
$$o_t = \sigma(w^o.[n^h_{t-1}, x_t] + b^o) \quad (5)$$
$$n^h_t = o_t * tanh(c_t) \quad (6)$$

The proposed forecasting model uses a M-LSTM network, which takes multiple inputs and predicts multiple output targets. The primary input features for the forecasting model include electricity price, demand and inflow, complemented by weather parameters such as temperature, wind speed, surface pressure, net solar radiation, net thermal radiation, dew point temperature, and precipitation. To enhance the forecast, additional external features are considered, including the hour of the day, day of the week, weekends, months, and seasons. The data processing phase involves addressing missing data, cleaning datasets, scaling data, and applying one-hot encoding to non-numerical data. The processed data are then fed into LSTM layers that include several hidden layers and a dropout layer to prevent overfitting. The architecture concludes with a dense layer, leading to an output layer that produces forecasts for target variables including; temperature, wind speed, electricity price, demand, etc. This approach allows for a more accurate prediction by accounting for the intricate interdependencies among the variables. The diagram of the proposed M-LSTM model is represented in Fig. 2.

2) Evaluation criteria: The performance and accuracy of forecasting models can be assessed through various evaluation metrics, each providing unique insights into the model's predictive accuracy. Among the commonly used metrics are mean absolute error (MAE), mean absolute percentage error (MAPE), and root mean squared error (RMSE) [26]. These metrics provide different perspectives on how well the model performs, highlighting errors, variability, and overall fit. In this study, the accuracy of the proposed forecasting model is evaluated primarily using MAPE and RMSE. However, for features that have low value ranges, close to zero, MAE is applied instead of MAPE. MAPE can yield misleading results for such features due to potential division by small or near-zero values, making it less appropriate in these cases. These metrics are presented in (7)–(9):

$$MAPE = \frac{100\%}{m} \sum_{i=1}^{m} \left| \frac{y_i - \hat{y}_i}{y_i} \right|, \quad (7)$$

$$RMSE = \sqrt{\frac{1}{m} \sum_{i=1}^{m} (y_i - \hat{y}_i)^2}, \quad (8)$$

$$MAE = \frac{1}{m} \sum_{i=1}^{m} |y_i - \hat{y}_i|, \quad (9)$$

where (y_i) and ($\hat{y}_i$) denote the actual and predicted values, respectively, and (m) denotes the number of predicted samples.

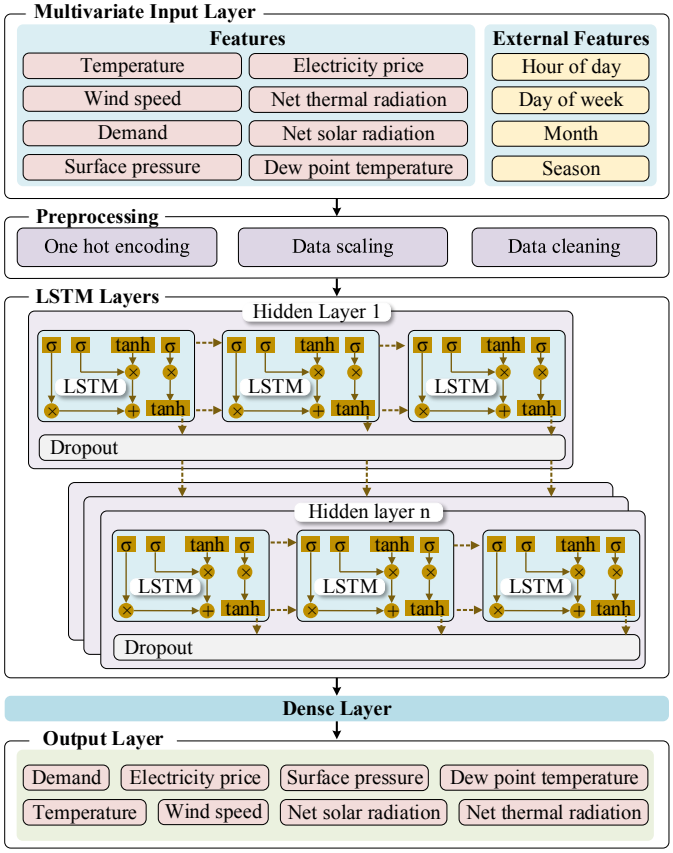

Fig. 2: Multivariate LSTM forecasting algorithm

B. Physics-Based Evaporation Model (PEM)

Accurate estimation of evaporation rates is essential for optimizing hydropower operations and maintaining reservoir levels. Higher temperatures will lead to increased evaporation and higher water loss from vegetation. The developed evaporation model calculates the hourly evaporation at hydropower reservoir locations. This model uses meteorological data including temperature, dewpoint temperature, wind speed, net radiation, ground heat flux, and atmospheric pressure. Reference evaporation for each reservoir area is estimated using Penman equation in (10)–(12), validated in many studies including [32]–[33]. The evaporation from each reservoir (12) is the sum of the radiative (10) and the aerodynamic (11) components [33]. The net radiation is a critical component of the surface energy balance, representing the difference between incoming and outgoing radiation at the Earth's surface, calculated in (13). Ground heat flux accounts for the heat exchange between the water surface and its surroundings. In this model, the ground heat flux is approximated based on the net radiation. This approximation is a simplified representation suitable for the context of open water surfaces where the ground heat flux can be considered similar to the heat exchange at the water surface. The calculation of ground heat flux is detailed in (14), where α^e is an empirical coefficient. When the net radiation

is positive (daytime), about 10% of it contributes to ground heat flux. Conversely, when the net radiation is negative (nighttime), approximately 50% contributes to ground heat flux, reflecting the cooling effect. Other essential parameters to calculate evaporation are saturation vapor pressure $e^s_{n,h,t}$ and actual vapor pressure $e^a_{n,h,t}$. The former defined in (15), represents the potential for air to hold moisture at a given temperature, while the latter, given in (16), measures the existing amount of water vapor in the air and is determined by the dewpoint temperature, which is the point at which air becomes saturated and condensation begins. Another crucial parameter in calculating evaporation is slope of the saturation vapor pressure curve. This parameter, represents the rate of change of the saturation vapor pressure with respect to temperature and is calculated in (17). To calculate evaporation, the u-component of the wind speed must be adjusted from the reservoir height (K^r) to the standard height of 2 meters above the surface (K^0). This adjustment is performed in (18) using the logarithmic law, a widely used analytical model for estimating the wind profile [34]. The roughness length denoted by Z^0 is a key parameter in the logarithmic law. It represents the height above the surface at which the wind speed theoretically becomes zero due to surface friction. For open water bodies like reservoirs, is typically small, e.g., 200 μm, reflecting the relatively smooth surface. The psychrometric constant in (19), accounts for the influence of air pressure and humidity on the evaporation.

$$E^R_{n,h,t} = \frac{a\Delta_{n,h,t}(R_{n,h,t} - G_{n,h,t})}{\Delta_{n,h,t} + \gamma_{n,h,t}(1 + \alpha\ u^s_{n,h,t})} \tag{10}$$

$$E^A_{n,h,t} = \frac{\gamma_{n,h,t}\frac{b}{T_{n,h,t}+c} u^s_{n,h,t}(e^s_{n,h,t} - e^a_{n,h,t})}{\Delta_{n,h,t} + \gamma_{n,h,t}(1 + \alpha\ u^s_{n,h,t})} \tag{11}$$

$$E^{ref}_{n,h,t} = E^R_{n,h,t} + E^A_{n,h,t} \tag{12}$$

$$R_{n,h,t} = SW^{\downarrow}_{n,h,t}(1 - \alpha^b) + LW^{\downarrow}_{n,h,t} - LW^{\uparrow}_{n,h,t} \tag{13}$$

$$G_{n,h,t} = \alpha^e R_{n,h,t} \tag{14}$$

$$e^s_{n,h,t} = e^0 \exp\left(\frac{\beta T_{n,h,t}}{T_{n,h,t} + T^0}\right) \tag{15}$$

$$e^a_{n,h,t} = e^0 \exp\left(\frac{\beta T^d_{n,h,t}}{T^d_{n,h,t} + T^0}\right) \tag{16}$$

$$\Delta_{n,h,t} = \frac{\Psi e^s_{n,h,t}}{(T_{n,h,t} + T^0)^2} \tag{17}$$

$$u^s_{n,h,t} = u^r_{n,h,t}\frac{\ln\left(\frac{K^0}{Z^0}\right)}{\ln\left(\frac{K^r}{Z^0}\right)} \tag{18}$$

$$\gamma_{n,h,t} = \frac{S^p_{n,h,t} C^p}{\epsilon^m L^v} \tag{19}$$

C. Long-term Hydropower Scheduling Problem

The objective of the long-term hydropower scheduling problem in (20) is to maximize the profit of the hydropower operator through participation in the day-ahead energy market. In this paper, the hydropower operator is considered a price taker, aiming to optimize decisions by participating in the day-ahead market and making direct sales to both public and private utilities. The profit is calculated by subtracting total operational costs from the total revenue generated through market participation and direct utility sales as follows:

$$\max \sum_{n\in\mathcal{N}}\sum_{t\in\mathcal{T}}\Bigg[\lambda^D_{n,t} p^{H,D}_{n,t} + \lambda^C_{n,t} P^{H,C}_{n,t} - l^{H,LS}_{n,t} - \sum_{h\in\mathcal{H}}(c^B_h q^B_{n,h,t} + c^S_h q^S_{n,h,t} + c^{SU}_h S^u_{n,h,t} + c^{SD}_h S^d_{n,h,t})\Bigg]. \tag{20}$$

The objective function in (20) is constrained to (21)–(38), presented next.

1) Cascade constraints: Long-term scheduling of cascade hydropower systems, where dams are hydraulically linked along a river, is a complex task due to upstream-downstream dependencies. Water releases from upstream reservoirs directly affect downstream availability, requiring coordinated operation to maximize overall power generation and profit across the system. The mathematical formulations provided in (21)–(26) outline the constraints associated with the topology of a cascaded system considering the management of water resources. The water inflow to each reservoir is equal to the sum of the outflow, spillage and the water bypass from the upstream reservoir, as formulated in (21). The net flow to the reservoir in (22) represents the balance between incoming and outgoing water flows. Incoming flow includes both release from upstream dams and natural inflow, while outgoing flow comprises outflow and water demand. Essentially, a portion of the reservoir's storage is utilized to satisfy water demands for purposes such as irrigation and drinking [35]. Total water released from reservoirs, which is the combined flow of bypassed, discharge and spilled water is represented in (23). Constraint (24) implies that the discharge from dams must lie within a specified range when the plant is on. The water bypassed, which is essential for preserving aquatic habitats, e.g., fish passage, is bounded in (25). The spillage water is bounded in (26) to avoid gas dissolution downstream.

$$q^{in}_{n,h,t} = \sum_{i\in\mathcal{I}_h} q^D_{n,i,t} + \sum_{i\in\mathcal{I}_h} q^S_{n,i,t} + \sum_{i\in\mathcal{I}_h} q^B_{n,i,t} \tag{21}$$

$$q^{net}_{n,h,t} = I_{n,h,t} + q^{in}_{n,h,t} - q^{out}_{n,h,t} - q^W_{n,h,t} \tag{22}$$

$$q^{out}_{n,h,t} = q^B_{n,h,t} + q^D_{n,h,t} + q^S_{n,h,t} \tag{23}$$

$$\underline{q^D_h} U_{n,h,t} \le q^D_{n,h,t} \le \overline{q^D_h} U_{n,h,t} \tag{24}$$

$$\underline{q^B_h} \le q^B_{n,h,t} \le \overline{q^B_h} \tag{25}$$

$$0 \le q^S_{n,h,t} \le \overline{q^S_h} \tag{26}$$

2) Water balance: The water balance, as detailed in (27), represents the equilibrium between the volume of water in reservoirs, accounting for the effects of evaporation, precipitation, and net flow [36]. The hourly volumetric rates of reservoir evaporation and precipitation are determined by multiplying the surface area of the reservoir by the hourly evaporation and precipitation rate in (28) and (29). The surface area of reservoirs $A_{n,h,t}$ is obtained from the global reservoir surface area dataset (GRSAD), which provides global reservoir data derived primarily from Earth observation satellite imagery [37]. The volume of each reservoir is bounded by an upper

limit to keep storage for flood control and a lower limit to preserve water for drought conditions (30).

$$V_{n,h,t} - V_{n,h,t-1} = q^{net}_{n,h,t}\delta + P^{v}_{n,h,t} - E_{n,h,t} : w^{v}_{n,h,t} \quad (27)$$

$$P^{v}_{n,h,t} = a^{c} P^{ref}_{n,h,t} A_{n,h,t} \quad (28)$$

$$E_{n,h,t} = a^{c} k_{c} E^{ref}_{n,h,t} A_{n,h,t} \quad (29)$$

$$\underline{V^{H}_{h}} \leq V_{n,h,t} \leq \overline{V^{H}_{h}} \quad (30)$$

3) Hydropower modeling: The dynamics of the water flow and the pressure head in a hydropower system is given by (31). The hydraulic head in (32) is defined as the difference between the average water level in the forebay and the tailwater at a given time [15]. The forebay water level is a function of the water volume as shown in (33). Also, tailwater level is influenced by the rate at which water is discharged from the hydro plant, indicated in (34). Accurate modeling of the tailwater level is crucial for assessing the downstream impact of hydro operations and for optimizing the overall performance of the cascade hydropower system. Functions represented in (33) and (34) are inherently non-linear and nonconvex, often modeled using higher-order polynomials. In this paper, these nonlinear relationships, including the HPF detailed in (31), are approximated using a piecewise linear regression-based machine learning approach. To effectively manage hydropower plant operations, the scheduling model must determine the optimal on/off status. According to (35), the output power of each hydropower plant lies within its minimum and maximum capacity limits when the plant is on. Constraint (36) ensures that if a plant transitions from off to on, it corresponds to a startup event. Conversely, if a plant transitions from on to off, it corresponds to a shutdown event. Constraint (37) ensures that a plant cannot start up and shut down simultaneously.

$$p^{H}_{n,h,t} = \eta_{h}\rho\ g\ q^{D}_{n,h,t} H^{D}_{n,h,t} \quad (31)$$

$$H^{D}_{n,h,t} = 1/2\ (Z^{f}_{n,h,t} + Z^{f}_{n,h,t-1}) - Z^{t}_{n,h,t} \quad (32)$$

$$Z^{f}_{n,h,t} = f^{f}_{h}(V_{n,h,t}) \quad (33)$$

$$Z^{t}_{n,h,t} = f^{t}_{h}(q^{D}_{n,h,t}) \quad (34)$$

$$\underline{P}_{h} U_{n,h,t} \leq p^{H}_{n,h,t} \leq \overline{P}_{h} U_{n,h,t} \quad (35)$$

$$S^{u}_{n,h,t} - S^{d}_{n,h,t} = U_{n,h,t} - U_{n,h,t-1} \quad (36)$$

$$S^{u}_{n,h,t} + S^{d}_{n,h,t} \leq 1 \quad (37)$$

4) Power balance: The total power generated from hydropower plants is intended to meet the annual demand as defined by contracts between hydropower operator and public and private utilities. Any surplus power can be sold in the market. In (38), the total power generated equals the sum of the contracted power and the power sold in the electricity market, and any power-balance shortfall is captured by the load shedding term.

$$\sum_{h \in \mathcal{H}} p^{H}_{n,h,t} = p^{H,D}_{n,t} + P^{H,C}_{n,t} - l^{H,LS}_{n,t} \quad (38)$$

D. Water Value Calculation

The water value, which represents the change in a hydropower operator's profit due to a marginal change in water storage volume, is crucial for decision-making regarding the use of water in hydropower reservoirs. Ignoring water value in day-ahead scheduling can lead to inefficient use of reservoir storage, potentially consuming resources, and resulting in suboptimal scheduling. This paper aims to calculate water values to provide hydropower operators with valuable insights for future resource management. Specifically, the water value determined by the proposed long-term scheduling model can be used as an input for day-ahead generation scheduling. In this paper, water values are determined using the dual variables (Lagrange multiplier) associated with the water balance constraint, represented by $w^{v}_{n,h,t}$ in (27) following the methodology outlined in [38]. To balance accuracy and computational efficiency, a deterministic optimization approach is employed. While this approach expedites calculations, adopting a stochastic approach in future research could further refine water value estimates taking into account uncertain operating conditions.

E. Piece-Wise Linearization Approach

To capture the nonlinear relationship between discharge flow, hydraulic head and hydropower production in a tractable manner, a piecewise linearization strategy is employed [39]. First, the set of observed $q^{D}_{n,h,t}$, $H^{D}_{n,h,t}$ data points is segmented into k distinct clusters using the K-means clustering algorithm. K-means clustering is an unsupervised machine learning algorithm that minimizes the sum of squared distances between data points and their corresponding centroids, thereby classifying the data into k clusters [40]. The optimal number of clusters is obtained using elbow method as outlined by [41]. Here, each K-means cluster's Voronoi region is approximated with an enclosing bounding box for simpler MILP encoding. Each cluster corresponds to a region Ω_k in the q^{D}, H^{D} plane. More explicitly, each cluster defines a subset of the joint domain of $(q^{D}_{n,h,t}, H^{D}_{n,h,t})$, denoted by Ω_k. Suppose that for cluster k we have breakpoints for discharge $\left(q^{\min}_{k,h}, q^{\max}_{k,h}\right)$ and for head $\left(H^{\min}_{k,h}, H^{\max}_{k,h}\right)$. Then, Ω_k is defined as:

$$\Omega_k = \Big\{ (q^{D}_{n,h,t},\ H^{D}_{n,h,t}) \Big|\ q^{\min}_{k,h} \leq\ q^{D}_{n,h,t} \leq\ q^{\max}_{k,h},\ H^{\min}_{k,h} \leq\ H^{D}_{n,h,t} \leq\ H^{\max}_{k,h} \Big\}. \quad (39)$$

Within each region Ω_k in (39), a linear function of the form (40) is applied. The Coefficients $\alpha_{h,k}, \beta_{h,k}$ and $\gamma_{h,k}$, which define the local linear relationship, are estimated via piecewise multiple linear regression [42]. Constraints (41) and (42) impose the piecewise linear relationship for the hydropower production $p^{H}_{n,h,t}$. When $u^{c}_{n,h,t,k} = 0$ for a given cluster k, the big-M technique effectively switches off that segment, so only the active cluster, i.e., $u^{c}_{n,h,t,k} = 1$, enforces its linear relation on $p^{H}_{n,h,t}$. Here, big-M denotes a sufficiently large positive constant M that relaxes the constraint whenever the segment is inactive. Constraint (43) restricts the discharge $q^{D}_{n,h,t}$ to the bounding box $(\, q^{\min}_{k,h},\, q^{\max}_{k,h})$ of the chosen cluster; if the plant is off, $q^{D}_{n,h,t}$ is forced to zero. Constraints (44)–(45) confine $H^{D}_{n,h,t}$ to the active cluster's range $(\, H^{\min}_{k,h},\, H^{\max}_{k,h})$ when plant is on and relax the bound to the global limits $(\underline{H^{D}_{h}}, \overline{H^{D}_{h}})$ when plant is off. This implies that even when the hydropower plant is off, the hydraulic head may remain

nonzero due to reservoir volume changes and inflow/outflow variations. Finally, constraint (46) ensures that exactly one cluster can be selected when the plant is on ($U_{n,h,t} = 1$) and no cluster is chosen when the plant is off ($U_{n,h,t} = 0$).

$$f^H_{n,h,t,k} = \alpha_{h,k} q^D_{n,h,t} + \beta_{h,k} H^D_{n,h,t} + \gamma_{h,k} \tag{40}$$

$$p^H_{n,h,t} \geq \sum_k \left(f^H_{n,h,t,k} - M(1 - u^c_{n,h,t,k}) \right) \tag{41}$$

$$p^H_{n,h,t} \leq \sum_k \left(f^H_{n,h,t,k} + M(1 - u^c_{n,h,t,k}) \right) \tag{42}$$

$$\sum_k q^{min}_{k,h} u^c_{n,h,t,k} \leq q^D_{n,h,t} \leq \sum_k q^{max}_{k,h} u^c_{n,h,t,k} \tag{43}$$

$$H^D_{n,h,t} \leq \sum_k H^{max}_{k,h} u^c_{n,h,t,k} + \overline{H^D_h}(1 - U_{n,h,t}) \tag{44}$$

$$H^D_{n,h,t} \geq \sum_k H^{min}_{k,h} u^c_{n,h,t,k} + \underline{H^D_h}(1 - U_{n,h,t}) \tag{45}$$

$$\sum_k u^c_{n,h,t,k} = U_{n,h,t} \tag{46}$$

Next, to implement piecewise linearization on (33) and (34), we partition the domains of $V_{n,h,t}$ and $q^D_{n,h,t}$ into $m^{'}$ and m breakpoints, shown by $V_1, V_2, \ldots, V_{m'}$ and $q_1, q_2, \ldots, q_m$, respectively. Each segment is then assigned a linear function with distinct coefficients, thereby describing the relationships between forebay water level and volume, as well as tailwater level and discharge flow, as shown in (47) and (48). A year long data for water volume and forebay level is used to predict $a^f_{h,m'}$ and $b^f_{h,m'}$ and data for discharge and tailwater level was used to approximate the coefficients $a^t_{h,m}$ and $b^t_{h,m}$. The model, trained on input-output data, captures this relationship by implementing a piecewise linear regression, effectively learning the underlying dynamics of the system in a data-driven manner. Additionally, the big-M method and binary variables, as introduced previously, are employed to allow the optimization problem to select one piecewise segment at a time and switch among segments when appropriate.

$$f^f_h(V_{n,h,t}) = \begin{cases} b^f_{h,1} + a^f_{h,1} V_{n,h,t}, & V_{n,h,t} \in [V_0, V_1) \\ b^f_{h,2} + a^f_{h,2} V_{n,h,t}, & V_{n,h,t} \in [V_1, V_2) \\ \vdots & \\ b^f_{h,m'} + a^f_{h,m'} V_{n,h,t}, & V_{n,h,t} \in [V_{m'-1}, V_{m'}]. \end{cases} \tag{47}$$

$$f^t_h(q^D_{n,h,t}) = \begin{cases} b^t_{h,1} + a^t_{h,1} q^D_{n,h,t}, & q^D_{n,h,t} \in [q_0, q_1) \\ b^t_{h,2} + a^t_{h,2} q^D_{n,h,t}, & q^D_{n,h,t} \in [q_1, q_2) \\ \vdots & \\ b^t_{h,m} + a^t_{h,m} q^D_{n,h,t}, & q^D_{n,h,t} \in [q_{m-1}, q_m]. \end{cases} \tag{48}$$

IV. Case Study

The proposed long-term scheduling framework is evaluated by comparing its performance against various cases and through analysis across five scenarios involving varying levels of extreme heat events. The proposed optimization problem is formulated as Mixed-Integer Linear Programming (MILP) problem and solved using CPLEX in GAMS on a desktop computer with a 4.0-GHz i7 processor and 32 GB of RAM. For benchmarking purposes, the corresponding mixed-integer nonlinear programming (MINLP) formulation is solved using DICOPT in GAMS on the same hardware configuration. The optimization is performed on an hourly basis throughout the year, ensuring that temporal variations in the market and hydropower operations are accurately captured. The M-LSTM model used data from 2016-2022 for training, reserving 2023 for testing. Two LSTM layers with 50 and 30 units are utilized. The first LSTM layer captures the initial temporal dependencies and passes to the second LSTM layer, which further refines the sequence patterns. The model is compiled with the Adam optimizer and uses the mean squared error as the loss function.

A. Data Description

The case study consists of 11 cascaded hydropower units including Grand Coulee, Chief Joseph, Wells, Rocky Reach, Rock Island, Wanapum, and Priest Rapids located in Washington State, and McNary, John Day, Dalles, and Bonneville dams located on the border between Washington and Oregon. The studied cascade hydropower system is shown in Fig. 3. The meteorological components of this study are derived from the ERA5-Land dataset, a comprehensive meteorological data set released by European Centre for medium-range weather forecasts [43]. The electricity price and demand data are derived from the California Independent System Operator [44]. The price for contracted energy sales have been sourced from the BPA's official documentation [45]. Hourly inflow data, as well as the technical parameters of the hydropower plants, such as generation capacity, are sourced from the Columbia river basin water management database, maintained by the Northwestern Division of the U.S. Army Corps of Engineers [46]. The three sets of simulation results, including the forecasting results, the PEM results, and the optimization results are presented next.

B. Results: Multivariate LSTM Forecasting

The M-LSTM model used in this study provides single-point predictions for the target variables. The performance of the model is measured using the evaluation metrics mentioned in Section III, and is shown in Table I. Figure 4 compares the daily average forecasted and actual values for some of the features such as wind speed, dew point temperature, temperature, solar radiation, electricity price, load, inflow, and precipitation. The load profile is relatively smooth without any sharp spikes. The precipitation pattern is slightly unpredictable, deviating from previous years due to its complex dynamics. Furthermore, the electricity price profile shows a spike during the summer, primarily driven by extreme heat events, consistent with trends observed in recent years despite the limited availability of long-term historical data. Overall, the M-LSTM model has effectively captured the patterns of these diverse features, delivering forecasts with acceptable levels of accuracy and error. The performance of the model demonstrates its ability to handle both stable and volatile variables, thus supporting its robustness in long-term scheduling under extreme heat events.

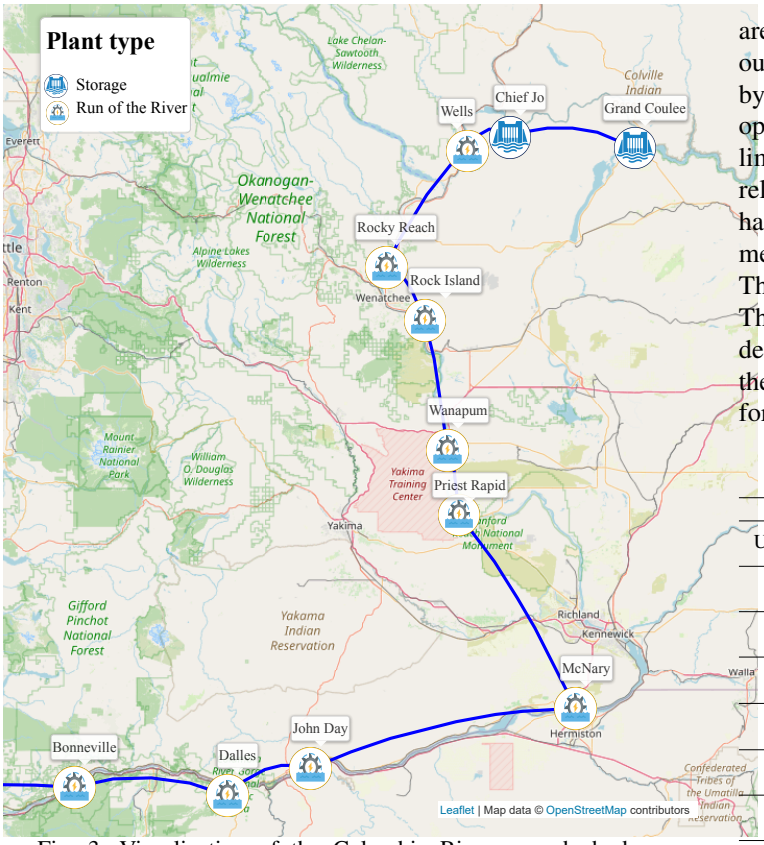

Fig. 3: Visualization of the Columbia River cascade hydropower system. Background map sourced from OpenStreetMap contributors.

Analyzing the performance of a forecasting algorithm requires evaluating its forecast value, as relying solely on quality-oriented metrics such as RMSE is insufficient [47]. To assess forecasting performance, two widely used time-series forecasting models are implemented and compared. The results are evaluated by running the scheduling model with actual data, representing perfect knowledge, as a benchmark. The profit generated by hydropower operators under each forecasting algorithm is determined, and the absolute profit deviation from perfect knowledge is calculated to assess the performance of the forecasting algorithms in terms of their economic value. Inspired by [48], the gated recurrent unit (GRU) is utilized. GRU is a type of recurrent neural network that addresses the vanishing gradient problem and enhances learning efficiency by employing gating mechanisms including reset and update gates. Additionally, the VARIMA is employed for further comparison [27]. VARIMA extends the classical ARIMA by handling multivariate time series, allowing it to model interdependencies between multiple variables. By incorporating both GRU and VARIMA, the analysis provides a robust comparison framework. GRU represents a deep learning-based approach adept at capturing non-linear and complex temporal relationships, while VARIMA offers a traditional statistical perspective that excels in modeling linear relationships and inter-variable dependencies. This dual comparison enables a comprehensive evaluation of the proposed M-LSTM's effectiveness in forecasting input parameters required for the hydropower scheduling problem. The results are summarized in Table II. The proposed M-LSTM model outperforms other forecasting approaches, VARIMA and GRU, by providing more accurate profit estimates for hydropower operators. VARIMA offers higher profit deviation indicates limitations in capturing the nonlinear and complex temporal relationships inherent in hydropower data. GRU's ability to handle nonlinear dependencies results in a significant improvement, while maintaining faster computational performance. The proposed M-LSTM model delivers the best performance. The computation time for M-LSTM is comparable to GRU, demonstrating its efficiency alongside superior accuracy. Here, the computation time is the sum of both optimization and forecasting times.

TABLE I: Forecasting accuracy for target features

Target Features	Performance Metric	Units	Value
U component of wind speed	RMSE	$[m/s]$	0.350
	MAPE	[%]	19.65
Dew point temperature	RMSE	$[k]$	0.742
	MAPE	[%]	0.19
Temperature	RMSE	$[k]$	0.768
	MAPE	[%]	0.21
Solar radiation	RMSE	$[j/m^2]$	357858
	MAPE	[%]	7.79
Thermal radiation	RMSE	$[j/m^2]$	226932
	MAPE	[%]	4.99
Surface pressure	RMSE	$[Pa]$	48.53
	MAPE	[%]	0.04
Electricity price	RMSE	$[\$/MWh]$	21.12
	MAPE	[%]	17.15
Load	RMSE	$[MW]$	474.08
	MAPE	[%]	1.44
Inflow	RMSE	$[kcfs]$	8.33
	MAPE	[%]	7.41
Precipitation	RMSE	$[mm]$	0.02
	MAE	$[mm]$	0.0144

TABLE II: Performance comparison of forecasting models in terms of profit, profit deviation, and computational time.

Forecast Model	Profit (Billion $)	Absolute Profit Deviation (%)	Computing Time (s)
VARIMA	14.994	17.59	269.66
GRU	16.825	7.52	236.71
Perfect Knowledge	18.195	—	109.05
Proposed	**18.758**	**3.09**	**239.29**

C. Results: Physics-Based Evaporation Model (PEM)

The proposed PEM is employed to estimate evaporation at the sites of storage hydropower plants, with the Grand Coulee Dam and Chief Joseph Dam, among the 11 cascaded plants, standing out as key storage reservoirs where this estimation is particularly critical. Figure 5 shows the model's performance in capturing evaporation trends over a 15-day period in August 2023, characterized by sustained high temperatures around $314\,\mathrm{K}$. This period is particularly noteworthy for its impact on evaporation rates due to the sustained high temperatures.Temperature and net radiation have been identified as the most influential parameters affecting the rate of evaporation. The data reveals a strong correlation between elevated temperatures and increased net radiation with higher rates of evaporation. During heat events, increased net radiation contributes to higher surface temperatures, thereby

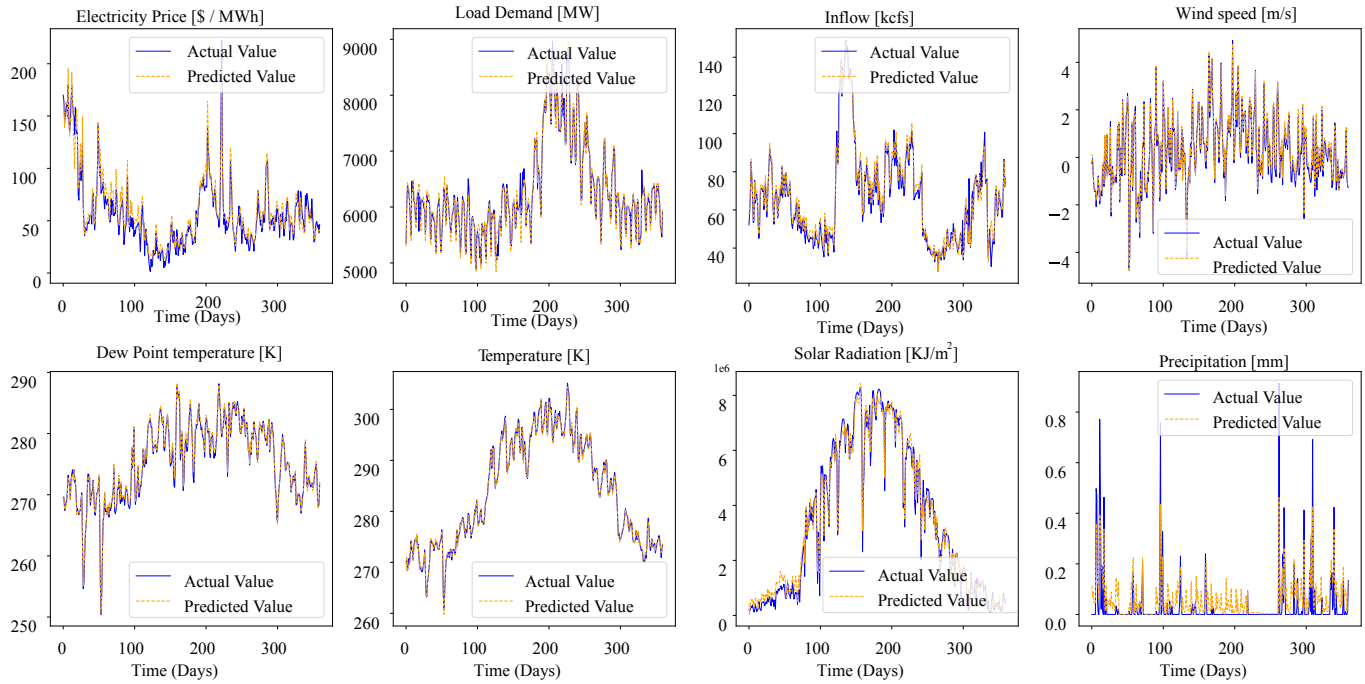

Fig. 4: Daily average actual and predicted values for target features.

enhancing the evaporation. Figure 6 illustrates the changes in evaporation and net radiation during 15 days.

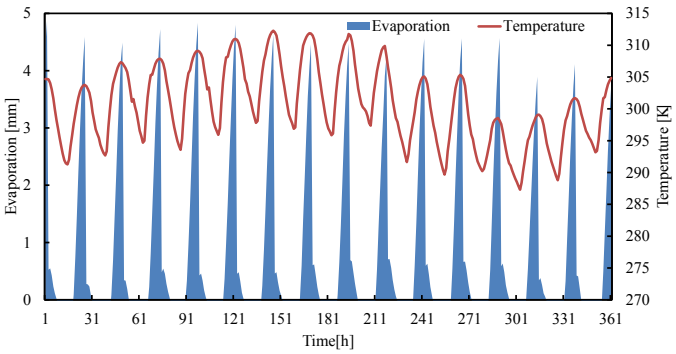

Fig. 5: Evaporation versus temperature trends over a 15-day period.

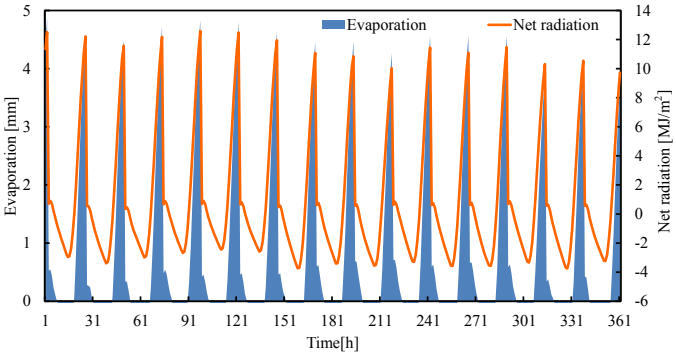

Fig. 6: Evaporation versus net radiation trends over a 15-day period.

D. Results: Long-Term Hydropower Scheduling

The hydropower plants operate strategically under long-term scheduling framework to not only meet demand but also maximize participation in the day-ahead market. This approach ensures that power generation aligns with market opportunities, to maximize profit. To this end, the hydropower operator conserves its water storage for periods when electricity prices are higher, thus maximizing its market participation during those times. Figure 7 illustrates the importance of long-term scheduling in this strategy. The total power generated is allocated to fulfill the contracted demand, with any surplus being sold in the day-ahead electricity market. To evaluate the effectiveness of the proposed long-term scheduling framework, its performance is compared across two cases (Cases 1 and 2), focusing on key metrics such as the profit obtained by hydropower operators and computational time, which reflects computational times for both forecasting and optimization tasks. This comparison highlights the necessity of incorporating PEM and the linearization of the hydropower production function (LHPF). The results are summarized in Table III, where the ”Modeling Features” column highlights the distinctions between the cases. For instance, the proposed model integrates PEM, the LHPF, and the M-LSTM for forecasting, showcasing a comprehensive approach to long-term hydropower scheduling. In contrast, Case 1 excludes the evaporation modeling component and LHPF from the proposed framework, simplifying the representation of water losses due to evaporation. Specifically, the nonlinear hydropower model is implemented through the constraint defined in (31), and polynomial regression is employed to represent the nonlinear functions presented in (33) and (34). The profit achieved by hydropower operators in Case 1 is higher than that in the proposed model because evaporation losses are not considered.

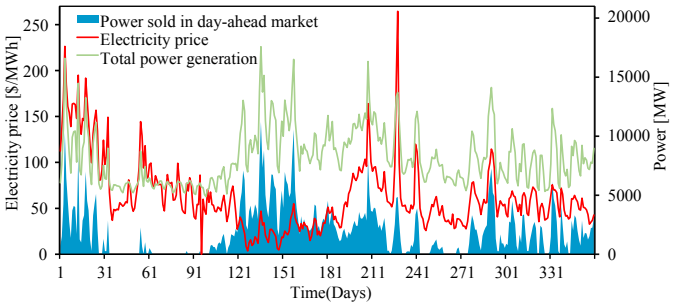

Fig. 7: Comparison of electricity price, total power generation, and power sold in the day-ahead market over a one-year period.

TABLE III: Comparison of the proposed long-term hydropower scheduling framework with other cases

Cases	Modeling Features			Profit	Computing
	PEM	Forecast model	LHPF	(Billion $)	Time(s)
Case 1	×	M-LSTM	×	18.980	559.06
Case 2	✓	M-LSTM	×	18.760	562.22
Proposed	✓	**M-LSTM**	✓	**18.758**	**239.29**

This highlights the significance of accounting for evaporation losses to provide a more realistic profit estimation for hydropower operators. Additionally, ignoring LHPF significantly increases computational time, as demonstrated in Case 1 and 2, due to the added complexity of solving a nonlinear optimization problem.

To further evaluate the proposed long-term scheduling model, five scenarios are applied over days 151–310 of the scheduling period. Each scenario simulates a severe heat period by demonstrating a specific temperature rise. Specifically, Scenarios 1, 2, 3, 4, and 5 represent temperature rises of 2°C, 4°C, 6°C, 8°C, and 10°C, respectively. To accurately capture the effects of temperature rise on electricity demand and prices, polynomial regression was employed to establish relationships between temperature and load, as well as temperature and price. This method quantifies the changes in demand and price associated with each 1°C increase in temperature. These relationships were used to create scenarios that realistically capture variations in demand and electricity prices, enabling a thorough evaluation of the model's performance under heatwave conditions. The water values associated with each scenario are depicted in Fig. 8, where Scenario 5 exhibits the highest water value during the summer period. This outcome is reasonable, as both electricity prices and demand reach their peak values during this time. Consequently, the model assigns a high water value to these periods to ensure that the hydropower operator reserves sufficient water in the reservoir. Figure 9 illustrates the storage volume associated with each scenario. The base case has the highest storage volume during the heat event, while Scenario 5, which is the most severe scenario, has the least. This is because Scenario 5 experiences the most extreme temperatures, leading to the highest evaporation rates and increased demand. Consequently, this results in less water being stored in the reservoirs. The market participation of the hydropower operator and total water stored in the dams across different scenarios is illustrated in Fig. 10, where the base case considers 100% participation. In Fig. 10, market participation in Scenario 5 is the lowest due to insufficient power generation during the extreme heat period. Despite high prices during this time, the reduced market participation highlights the adverse market conditions caused by extreme heat events. Elevated temperatures significantly increase evaporation rates, reducing water availability in reservoirs and subsequently limiting the hydropower generation capacity. Furthermore, the increased demand during heatwaves further constrains the capacity available for market participation. Even with the potential for higher revenue, the hydropower operator struggles to participate more in the market due to the limited power generation capacity. These findings highlight the challenging and often unfavorable conditions in electricity markets during extreme events.

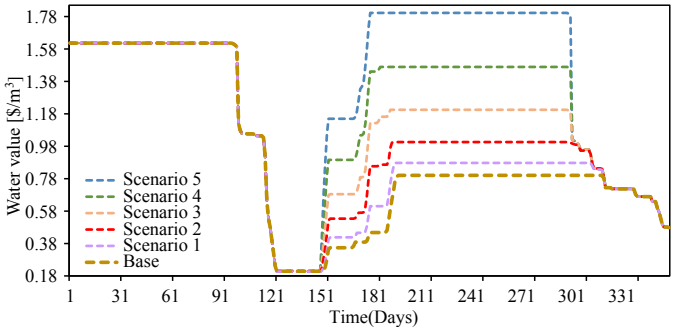

Fig. 8: Value of water in storage for different scenarios.

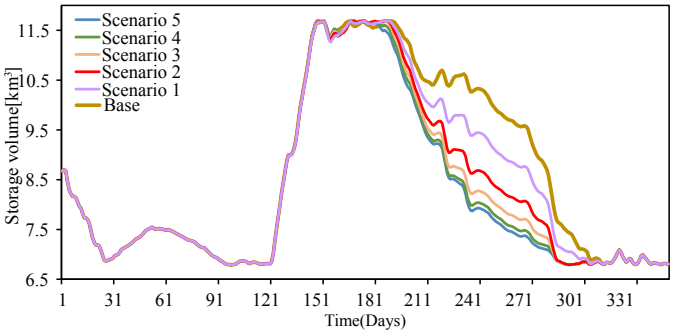

Fig. 9: Reservoir storage volumes for different scenarios.

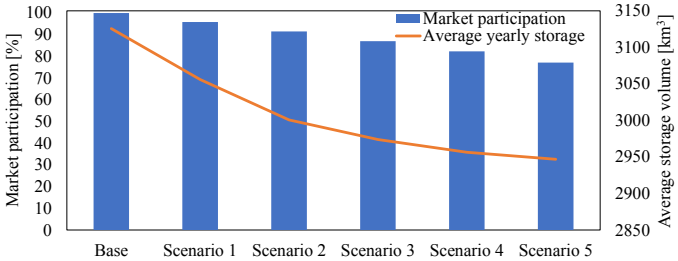

Fig. 10: Day-ahead market participation and average yearly storage for different scenarios compared with base case.

V. Conclusion

This paper presented an integrated artificial intelligence and physics-based modeling framework for long-term scheduling

of hydropower under various extreme heat scenarios, focusing on maximizing the profit of the hydropower operator. By integrating a physics-based evaporation model and multivariate LSTM forecasting technique, the study improved the accuracy of long-term scheduling, addressing key challenges posed by extreme heat events. The regression-based machine learning technique was used to transform the non-linear and non-convex behavior of the hydropower generation function into a mixed integer linear formulation. The results demonstrated the effectiveness of the proposed long-term scheduling framework in enhancing market participation during extreme events. The performance of the model was evaluated against various cases, each highlighting the significance of specific components within the framework. These comparisons underscored the limitations of alternative approaches, such as models that lack evaporation modeling, higher computational time due to nonlinear hydropower modeling, or rely on alternative forecasting methods like VARIMA and GRU. Notably, the proposed framework achieved profits closest to those obtained with perfect knowledge, further validating its efficiency and robustness. Additionally, the water values derived from the proposed framework emerge as a strategic tool, can empower operators to make more informed short-term scheduling decisions. While the formulation in this paper employs a deterministic approach to ensure computational tractability, future research may include exploring stochastic optimization methods to explicitly incorporate uncertainty in inflow, demand and market prices in the long-term scheduling problem.

REFERENCES

[1] Z. Chen, J. Lu, C.-C. Chang, S. W. Lubis, and L. R. Leung, "Projected increase in summer heat-dome-like stationary waves over northwestern north america," *npj Climate and Atmospheric Science*, vol. 6, no. 1, p. 194, 2023.

[2] M. A. Larsen, S. Petrović, A. M. Radoszynski, R. McKenna, and O. Balyk, "Climate change impacts on trends and extremes in future heating and cooling demands over europe," *Energy and Buildings*, vol. 226, p. 110397, 2020.

[3] A. Farley, H. Belnap, and M. Parvania, "Resilience hubs: Bolstering the grid and empowering communities," *IEEE Power and Energy Magazine*, vol. 22, no. 4, pp. 38–48, 2024.

[4] M. Baghkarvasef, M. Majidi, and M. Parvania, "Dynamic modeling and real-time control of hydropower units for frequency regulation," in *2024 IEEE PES Innovative Smart Grid Technologies Conference (ISGT)*, 2024, pp. 1–5.

[5] B. Boehlert, K. M. Strzepek, Y. Gebretsadik, R. Swanson, A. McCluskey, J. E. Neumann, J. McFarland, and J. Martinich, "Climate change impacts and greenhouse gas mitigation effects on us hydropower generation," *Applied Energy*, vol. 183, pp. 1511–1519, 2016.

[6] Z. Sun, Z. Ouyang, J. Zhao, S. Li, X. Zhang, and W. Ren, "Recent rebound in observational large-pan evaporation driven by heat wave and droughts by the lower yellow river," *Journal of hydrology*, vol. 565, pp. 237–247, 2018.

[7] K. Friedrich, R. L. Grossman, J. Huntington, P. D. Blanken, J. Lenters, K. D. Holman, D. Gochis, B. Livneh, J. Prairie, E. Skeie *et al.*, "Reservoir evaporation in the western united states: current science, challenges, and future needs," *Bulletin of the American Meteorological Society*, vol. 99, no. 1, pp. 167–187, 2018.

[8] V. Penmetsa and K. E. Holbert, "Climate change effects on solar, wind and hydro power generation," in *2019 North American Power Symposium (NAPS)*, 2019, pp. 1–6.

[9] L. Rodriguez-Garcia, M. Heleno, and M. Parvania, "Power distribution system planning for mitigating overheating risk inequity," *IEEE Transactions on Power Systems*, vol. 40, no. 1, pp. 920–932, 2025.

[10] A. Farley, H. Belnap, and M. Parvania, "Siting and sizing resilience hubs for grid and community resilience during heat waves," in *2025 58th Hawaii International Conference on System Sciences (HICSS)*, 2025, pp. 2946–2955.

[11] A. Alawad, A. Alnakhli, and P. Dehghanian, "Optimal energy management of a power transmission grid under a heatwave exposure," in *2021 North American Power Symposium (NAPS)*, 2021, pp. 1–6.

[12] X. Ke, D. Wu, J. Rice, M. Kintner-Meyer, and N. Lu, "Quantifying impacts of heat waves on power grid operation," *Applied energy*, vol. 183, pp. 504–512, 2016.

[13] A. Pechan and K. Eisenack, "The impact of heat waves on electricity spot markets," *Energy Economics*, vol. 43, pp. 63–71, 2014.

[14] C. Ø. Naversen, M. Parvania, A. Helseth, and H. Farahmand, "Continuous hydrothermal flexibility coordination under wind power uncertainty," *IEEE Transactions on Sustainable Energy*, vol. 13, no. 4, pp. 1900–1912, 2022.

[15] C. Wang, P. Ju, C. Wan, F. Wu, S. Lei, X. Pan, and T. Lu, "Resilience-based coordinated scheduling of cascaded hydro power with sequential heavy precipitation," *IEEE Transactions on Sustainable Energy*, vol. 14, no. 2, pp. 1299–1311, 2022.

[16] H. Wang, S. Liao, B. Liu, H. Zhao, X. Ma, and B. Zhou, "Long-term complementary scheduling model of hydro-wind-solar under extreme drought weather conditions using an improved time-varying hedging rule," *Energy*, vol. 305, p. 132285, 2024.

[17] A. R. de Queiroz, L. M. M. Lima, J. W. M. Lima, B. C. da Silva, and L. A. Scianni, "Climate change impacts in the energy supply of the brazilian hydro-dominant power system," *Renewable energy*, vol. 99, pp. 379–389, 2016.

[18] V. Espanmanesh and A. Tilmant, "Optimizing the management of multireservoir systems under shifting flow regimes," *Water Resources Research*, vol. 58, no. 6, p. e2021WR030582, 2022.

[19] P. Qin, H. Xu, M. Liu, C. Xiao, K. E. Forrest, S. Samuelsen, and B. Tarroja, "Assessing concurrent effects of climate change on hydropower supply, electricity demand, and greenhouse gas emissions in the upper yangtze river basin of china," *Applied Energy*, vol. 279, p. 115694, 2020.

[20] V. Espanmanesh, E. Guilpart, M.-A. Bourgault, and A. Tilmant, "Adapting reservoir operation to climate change in regions with long-term hydrologic persistence," *Climate Risk Management*, p. 100623, 2024.

[21] Z. He, J. Zhou, H. Qin, B. Jia, F. He, G. Liu, and K. Feng, "A fast water level optimal control method based on two stage analysis for long term power generation scheduling of hydropower station," *Energy*, vol. 210, p. 118531, 2020.

[22] A. L. Diniz, F. D. S. Costa, M. E. Maceira, T. N. dos Santos, L. C. B. Dos Santos, and R. N. Cabral, "Short/mid-term hydrothermal dispatch and spot pricing for large-scale systems-the case of brazil," in *2018 Power Systems Computation Conference (PSCC)*, 2018, pp. 1–7.

[23] J. Barzola-Monteses, J. Gómez-Romero, M. Espinoza-Andaluz, and W. Fajardo, "Time series forecasting techniques applied to hydroelectric generation systems," *International Journal of Electrical Power & Energy Systems*, vol. 164, p. 110424, 2025.

[24] Z. C. Herbert, Z. Asghar, and C. A. Oroza, "Long-term reservoir inflow forecasts: Enhanced water supply and inflow volume accuracy using deep learning," *Journal of Hydrology*, vol. 601, p. 126676, 2021.

[25] S. Buhan, D. Küçük, M. S. Cinar, U. Güvengir, T. Demirci, Y. Yilmaz, F. Malkoc, E. Eminoğlu, and M. U. Yildirim, "A scalable river flow forecast and basin optimization system for hydropower plants," *IEEE Transactions on Sustainable Energy*, vol. 11, no. 4, pp. 2220–2229, 2019.

[26] P. Malhan and M. Mittal, "A novel ensemble model for long-term forecasting of wind and hydro power generation," *Energy Conversion and Management*, vol. 251, p. 114983, 2022.

[27] Y. Zhang, C. Cheng, R. Cao, G. Li, J. Shen, and X. Wu, "Multivariate probabilistic forecasting and its performance's impacts on long-term dispatch of hydro-wind hybrid systems," *Applied Energy*, vol. 283, p. 116243, 2021.

[28] Z. Wei, X. Shen, G. Qiu, Y. Liu, and J. Liu, "An integrated transfer learning method for power generation prediction of run-off small hydropower in data-scarce areas," *IEEE Transactions on Smart Grid*, vol. 15, no. 1, pp. 1030–1041, 2023.

[29] N. Sevang, "Long-term hydropower scheduling using scenario reduction and short-term inflow prediction," Master's thesis, Norwegian University of Science and Technology (NTNU), 2023, master's Thesis. [Online]. Available: https://ntnuopen.ntnu.no/ntnu-xmlui/handle/11250/3153313

[30] R. Uría-Martínez, M. Johnson, P. O'Connor, N. M. Samu, A. M. Witt, H. Battey, T. Welch, M. Bonnet, and S. Wagoner, "2017 hydropower market report," Oak Ridge National Laboratory (ORNL), Oak Ridge, TN (United States). Oak ..., Tech. Rep., 2018.

[31] D. G. Miralles, P. Gentine, S. I. Seneviratne, and A. J. Teuling, "Land–atmospheric feedbacks during droughts and heatwaves: state of the science and current challenges," *Annals of the New York Academy of Sciences*, vol. 1436, no. 1, pp. 19–35, 2019.
[32] T. McMahon, M. Peel, L. Lowe, R. Srikanthan, and T. McVicar, "Estimating actual, potential, reference crop and pan evaporation using standard meteorological data: a pragmatic synthesis," *Hydrology and Earth System Sciences*, vol. 17, no. 4, pp. 1331–1363, 2013.
[33] W. Tian, X. Liu, K. Wang, P. Bai, C. Liu, and X. Liang, "Estimation of global reservoir evaporation losses," *Journal of Hydrology*, vol. 607, p. 127524, 2022.
[34] G. Gualtieri and S. Secci, "Methods to extrapolate wind resource to the turbine hub height based on power law: A 1-h wind speed vs. weibull distribution extrapolation comparison," *Renewable Energy*, vol. 43, pp. 183–200, 2012.
[35] M. Elsir, A. T. Al-Awami, M. A. Antar, K. Oikonomou, and M. Parvania, "Risk-based operation coordination of water desalination and renewable-rich power systems," *IEEE Transactions on Power Systems*, vol. 38, no. 2, pp. 1162–1175, 2022.
[36] W. Wan, H. Wang, and J. Zhao, "Hydraulic potential energy model for hydropower operation in mixed reservoir systems," *Water Resources Research*, vol. 56, no. 4, p. e2019WR026062, 2020.
[37] H. Gao and G. Zhao, "Global Reservoir Surface Area Dataset (GRSAD)," 2019. [Online]. Available: https://doi.org/10.18738/T8/DF80WG
[38] S. Wang, J. Liu, R. Bo, and Y. Chen, "Approximating input-output curve of pumped storage hydro plant: A disjunctive convex hull method," *IEEE Transactions on Power Systems*, vol. 38, no. 1, pp. 63–74, 2022.
[39] J. A. Warwicker and S. Rebennack, "Efficient continuous piecewise linear regression for linearising univariate non-linear functions," *IISE Transactions*, pp. 1–15, 2024.
[40] M. Fan, Z. Li, T. Ding, L. Huang, F. Dong, Z. Ren, and C. Liu, "Uncertainty evaluation algorithm in power system dynamic analysis with correlated renewable energy sources," *IEEE Transactions on Power Systems*, vol. 36, no. 6, pp. 5602–5611, 2021.
[41] A. Radovanovic, T. Nesti, and B. Chen, "A holistic approach to forecasting wholesale energy market prices," *IEEE Transactions on Power Systems*, vol. 34, no. 6, pp. 4317–4328, 2019.
[42] S. Chen, X. Zhou, G. Zhou, C. Fan, P. Ding, and Q. Chen, "An online physical-based multiple linear regression model for building's hourly cooling load prediction," *Energy and buildings*, vol. 254, p. 111574, 2022.
[43] J. Muñoz-Sabater, E. Dutra, A. Agustí-Panareda, C. Albergel, G. Arduini, G. Balsamo, S. Boussetta, M. Choulga, S. Harrigan, H. Hersbach *et al.*, "Era5-land: A state-of-the-art global reanalysis dataset for land applications," *Earth system science data*, vol. 13, no. 9, pp. 4349–4383, 2021.
[44] California ISO, "Oasis market results interface," http://oasis.caiso.com/mrioasis/logon.do?reason=application.baseAction.noSession, 2024.
[45] Bonneville Power Administration, "Power rates," 2024. [Online]. Available: https://www.bpa.gov/energy-and-services/rate-and-tariff-proceedings/power-rates
[46] U.S. Army Corps of Engineers (USACE), "Dataquery interface for hydrological data," https://www.nwd-wc.usace.army.mil/dd/common/dataquery/www/, 2024.
[47] J. Zhong, X. Lei, Z. Shao, and L. Jian, "A reliable evaluation metric for electrical load forecasts in v2g scheduling considering statistical features of ev charging," *IEEE Transactions on Smart Grid*, 2024.
[48] X. Zhang, T. K. Chau, Y. H. Chow, T. Fernando, and H. H.-C. Iu, "A novel sequence to sequence data modelling based cnn-lstm algorithm for three years ahead monthly peak load forecasting," *IEEE Transactions on Power Systems*, vol. 39, no. 1, pp. 1932–1947, 2023.

Maryam Baghkarvasef (S' 2022) received the B.Sc. degree in Electrical Engineering from University of Tabriz in 2022 and the M.Sc. degree in Electrical Engineering from the University of Utah in 2025, where she is currently pursuing the Ph.D. degree in Electrical Engineering. Her research interests include the application of optimization and machine learning techniques for modeling and scheduling of hydropower and hybrid energy storage resources, and the resilience of power systems under extreme weather events.

Masood Parvania (SM' 2019) is the Roger P. Webb Professor of Electrical and Computer Engineering and the Director of Utah Smart Energy Laboratory at the University of Utah. His research interests include the operation, economics, and resilience of power and energy systems, as well as modeling and operation of interdependent critical infrastructures. Dr. Parvania currently serves as an Associate Editor for the IEEE Transactions on Power Systems.